Electronic structure robustness and design rules for 2D colloidal heterostructures

Audrey Chu, Clément Livache, Sandrine Ithurria, Emmanuel Lhuillier

Electronic structure robustness and design rules for 2D colloidal heterostructures

Audrey Chu, Clément Livache, Sandrine Ithurria, and Emmanuel Lhuillier

Electronic structure robustness and design rules for 2D colloidal heterostructures

Audrey Chu,[1,2] Clément Livache,[1,2] Sandrine Ithurria,[2,a)] and Emmanuel Lhuillier[1,a)]

[1]*Sorbonne Universités, UPMC Univ. Paris 06, CNRS-UMR 7588, Institut des NanoSciences de Paris, 4 place Jussieu, 75005 Paris, France*
[2]*Laboratoire de Physique et d'Etude des Matériaux, ESPCI-ParisTech, PSL Research University, Sorbonne Université UPMC Univ Paris 06, CNRS, 10 rue Vauquelin, 75005 Paris, France*

Among the colloidal quantum dots, 2D nanoplatelets present exceptionally narrow optical features. Rationalizing the design of heterostructures of these objects is of utmost interest; however, very little work has been focused on the investigation of their electronic properties. This work is organized into two main parts. In the first part, we use 1D solving of the Schrödinger equation to extract the effective masses for nanoplatelets (NPLs) of CdSe, CdS, and CdTe and the valence band offset for NPL core/shell of CdSe/CdS. In the second part, using the determined parameters, we quantize how the spectra of the CdSe/CdS heterostructure get affected by (i) the application of an electric field and (ii) by the presence of a dull interface. We also propose design strategies to make the heterostructure even more robust. *Published by AIP Publishing.* https://doi.org/10.1063/1.5003289

I. INTRODUCTION

Among nanocrystals, 2D nanoplatelets[1–3] (NPLs) of cadmium chalcogenides have generated significant interest, thanks to the lack of inhomogeneous broadening in the luminescent signal.[4] This results from the absence of roughness in the only confined direction.[5] In addition to their narrow linewidth, NPLs are also an interesting platform for low threshold lasing,[6–8] photodetection,[9,10] and field effect transistors.[11] However, far less work has been focused on the investigation of their electronic structure[12,13] and, in particular, once heterostructures are grown.[14] This results from the lack of band structure parameters for II–VI semiconductor compounds that prevents advanced modelisation of those materials as it has been conducted for devices based on heterostructures of III–V materials (quantum well infrared photodetectors,[15,16] quantum cascade lasers,[17] and detectors[18]).

2D NPLs with confinement only along their thickness are an interesting platform to tackle this challenge since only 1D modeling is necessary. Until now, the modeling of the electronic spectrum of the 2D NPL[19–21] has been conducted using several approaches which include the k·p method,[12] tight binding,[13,22] and the shooting method.[14,23,24] While the first two methods are well suited for homomaterials, their use for heterostructures[25] is not straightforward and more effective approaches are necessary. However, from an applied perspective, these heterostructures drive the interest for this type of nanocrystal due to their high photoluminescence efficiency and improved stability. This is especially true since the recent introduction of high-temperature grown shells for 2D NPL.[14,26,27]

In this paper, we are addressing the effect of a non-ideal band profile on the electronic properties of 2D cadmium chalcogenides NPL. Typically, we aim at quantifying the impact of effects such as (i) the presence of an electric field and (ii) the growth of non-sharp interfaces (i.e., gradient interfaces).

The paper is organized as follows: We first synthesized a series of CdSe, CdS, and CdTe NPLs as well as CdSe/CdS NPLs with different thicknesses and used the measured spectra as input to determine the effective masses and material band offsets. In a second time, we used the determined parameters to quantify the effect of the non-ideal band profile on the electronic spectrum of a 2D CdSe/CdS NPL.

II. EXPERIMENTAL SECTION

A. Chemicals

Cadmium nitrate tetrahydrate $[Cd(NO_3)_2(H_2O)_4]$ (Aldrich 99,999%), Cadmium acetate dihydrate $[Cd(OAc)_2(H_2O)_2]$ (Aldrich 98%), Cadmium oxide (Strem, 99.99%), Tellurium Powder (Aldrich, 99.99%), Selenium Powder (Strem chemical, 99.99%), Sulfur Powder (Aldrich, 99.98%), $NaBH_4$ (Aldrich, 98%), n-Hexane (Carlo Erba, 95%), Ethanol (Carlo Erba, 99.9%, EtOH), Methanol (Carlo Erba, 99.9%, MeOH), n-Methyl-Formamide (Aldrich, 99%, NMF), Octadecene (Aldrich, 90%, ODE), Toluene (Carlos Erba, 99.8%), Oleic acid (Aldrich, 90%, OA), Octylamine (Aldrich, 99%), Na_2S (sigma-Aldrich, 99.5%), Myristic Acid (sigma-Aldrich, >99%), tri-Buthylphosphine (Aldrich, 97%, TBP), Tri-Octylphosphine (Aldrich, 97%, TOP), and Oleylamine (Achros, 80%–90%, OLA) were used.

B. Nanoplatelet synthesis

1. Synthesis of 4 monolayer (ML) CdS NPLs[42]

In a three-neck flask, 160 mg of $Cd(OAc)_2(H_2O)_2$, 1.5 mL of a solution at 0.1 M of S in ODE, 0.17 g of OA, and 9 mL of ODE are introduced and degassed. Under argon, the temperature is raised to 260 °C in 15 min. The system is kept

a)Authors to whom correspondence should be addressed: sandrine.ithurria@espci.fr and el@insp.upmc.fr

at 260 °C for a minute then the heating mantle is removed. NPLs are precipitated with a mixture of hexane and ethanol. The NPLs are suspended in 10 mL of hexane.

2. Synthesis of 4 MLs CdSe NPLs

In a 50 mL three-neck flask, 340 mg of Cd(myr)$_2$, 24 mg of selenium, and 25 mL of ODE are introduced and degassed for 30 min at room temperature. Then, the mixture is put under argon flow, and the temperature is raised to 240 °C. When the mixture reaches 200 °C, 110 mg of Cd(OAc)$_2$(H$_2$O)$_2$ are introduced. The reaction is stopped after 10 min at 240 °C. The NPLs are precipitated through the addition of a mixture of 30 mL of hexane and 30 mL of EtOH. The NPLs are suspended in 10 mL of hexane.

3. Synthesis of 3 ML CdSe NPLs

In a three-neck flask, 240 mg of Cd(OAc)$_2$(H$_2$O)$_2$, 150 μL of oleic acid, and 15 mL of ODE are degassed under vacuum for 45 min at 80 °C. Then, under argon flow, the mixture is heated up to 195 °C. 150 μl of TOPSe at 1 M is swiftly injected. After 40 min of reaction, the mixture is cooled down and precipitated with ethanol. The NPLs are suspended in 10 mL of hexane.

4. Synthesis of 4 ML CdTe

In a three-neck flask, 133.3 mg of Cd(OAc)$_2$(H$_2$O)$_2$ (0.5 mmol), 80 μL of OA, and 10 mL of ODE are introduced and degassed for 2 h at 95 °C. Then, under argon, the temperature is increased to 210 °C. When the temperature is between 170 °C and 190 °C, a solution of TOP-Te is swiftly added (100 μL of TOP-Te, 1 M, diluted in 0.5 mL of ODE). The reaction is stopped after 30 min at 210 °C by adding 1 mL of OA. At room temperature, NPLs are precipitated through the addition of a mixture of hexane and EtOH. The NPLs are suspended in 10 mL of hexane.

C. Thick and heterostructure platelet synthesis

In order to grow thicker NPLs or to grow heterostructured (CdSe/CdS) NPLs, we use the C-ALD procedure, described in Ref. 30. The procedure allows to grow the material layer by layer (i.e., at each step, the NPL thickness increases by half a lattice parameter). In the case of CdS growth, we use the following procedure: 1 mL of synthesised NPLs is precipitated with ethanol and suspended in 2 mL of hexane. Then, 2 mL of NMF are added in order to form a biphasic mixture. 100 μL of a solution of Na$_2$S and 9H$_2$O at 0.1 M in NMF are added to the mixture and stirred up to a complete transfer of the NPLs in the polar phase. 10 μL of TBP are then added to complex all the polysulfide. The NPLs in NMF are rinsed twice with a mixture of 2 mL of hexane and 20 μL of EtOH. Then, the NPLs are precipitated with toluene and suspended in 2 mL of NMF. The other half monolayer is grown through the addition of 100 μL of a solution of Cd(OAc)$_2$(H$_2$O)$_2$ at 0.1 M in NMF. After stirring, the NPLs are transferred back in a non-polar phase by the addition of 2 mL of hexane on top of NMF and 20 μL of OLA. Methanol can be added to facilitate the NPL transfer and the

phase separation. The NPLs suspended in 3 mL of ODE, 25 mg of Cd(OAc)$_2$(H$_2$O)$_2$, 35 μL of OA, and 35 μL of TBP are introduced in a three neck flask. After degassing for 15 min at room temperature, the flask is put under argon flow and heated at 230 °C for 30 min until the optical features gets refined. Then, the NPLs are precipitated with ethanol and suspended in hexane. The same process is reproduced for each additional layer.

In the case of CdSe growth, we use the following Selenide solution: 20 mg of NaBH$_4$ are dissolved in 0.5 mL of NMF and 0.5 mL of EtOH. Then, 12 mg of selenium powder sonicated in 0.5 mL of NMF is slowly added to the solution of NaBH$_4$. NaBH$_4$ will reduce the selenium powder in Se^{2-} with the degassing of H$_2$. After 10 min, the reaction should be complete and the solution colorless. In the case of CdTe, the procedure is the same as for Se, while replacing the Se by Te powder. It is also worth pointing that the reaction needs to be conducted in an air free glove box in the case of CdTe to prevent the oxidation of Te^{2-}.

D. Material characterization

The absorption spectra are acquired for NPLs in dilute solution using a Shimadzu UV 3600 plus. For electron microscopy imaging, the same solution of NPLs diluted in hexane is drop-cast on a TEM grid and degassed overnight. Images are acquired at 200 kV using a JEOL 2010 microscope.

III. NUMERICAL SIMULATION

The 1D time-independent Schrödinger equation is

$$\left[-\frac{\hbar^2}{2}\frac{d}{dz}\frac{1}{m^*(z)}\frac{d}{dz} + V(z) \right]\xi(z) = E\xi(z), \qquad (1)$$

with $\hbar$ the reduced Planck constant, m*(z) the effective mass of the band, V(z) the band profile, E the eigen-energy, and ξ the wavefunction. This equation is discretized and the wavefunction can be evaluated at any step knowing its value at the two earlier steps according to the following equation:

$$\frac{\xi(z+dz)}{m^*\left(z+\frac{dz}{2}\right)} = \left[\frac{2}{\hbar^2}dz^2(V(z)-E) + \frac{1}{m^*\left(z+\frac{dz}{2}\right)} \right.$$
$$\left. + \frac{1}{m^*\left(z-\frac{dz}{2}\right)} \right]\xi(z) - \frac{\xi(z-dz)}{m^*\left(z-\frac{dz}{2}\right)}. \qquad (2)$$

The typical discretization step is 0.1 nm. We then inject the limit condition $\xi(0) = 0$ which means that the wavefunction is null outside of the confined structure. We then set $\xi(1)$ = 1 or any non-null value. Its exact value will actually be determined by the wavefunction normalization. We evaluate the wavefunction at all energies between the bottom of the band and the vacuum offset. Among all the energies, the eigen energies are the one which minimize the value of $|\xi(L)|$, where L is the length of the structure. Any other solution is non-physical. The eigen spectrum is basically obtained by looking at the change of sign of $\xi(L)$ as a function of the

energy, as illustrated in Fig. S1 (supplementary material). This numerical resolution of the Schrödinger equation is called shooting method and is extensively discussed in Harrison's book.[24] In such a model, band non parabolocity, effect of strain (due to ligands[28] or shell growth), and dielectric confinement[13] are not considered.

IV. RESULTS AND DISCUSSION

A. Determination of the effective masses and band offsets

We first colloidally grow a series of CdSe, CdS, and CdTe[29] NPLs with different thicknesses, as well as CdSe/CdS core shell platelets with 4 monolayers of CdSe and various shell thicknesses[30] (4 monolayer NPLs means 5 planes of cadmium alternated with 4 planes of selenide in the [001] direction of the zinc blend structure). The procedures are given in Sec. II. The associated spectra are given in Figs. 1(a), 1(b), and S2 (supplementary material). Table S1 (supplementary material) gives the first and second exciton energies for these materials. In NPLs, these two excitons correspond to the heavy hole to conduction band transition (lowest energy transition) and to the light hole to conduction band transition.[12] Moreover, it was already discussed that in such 2D NPLs, the exciton binding energy is balanced by the self-energy term and that finally the quantum confinement term is leading to the main correction of the band edge energy.[13] As a result, the band-edge energy can be obtained by summing the hole and electron confinement energies to the bulk band gap. In the following, we numerically solve the 1D Schrödinger equation given by Eq. (2). Table I provides the material parameters used for the simulation.
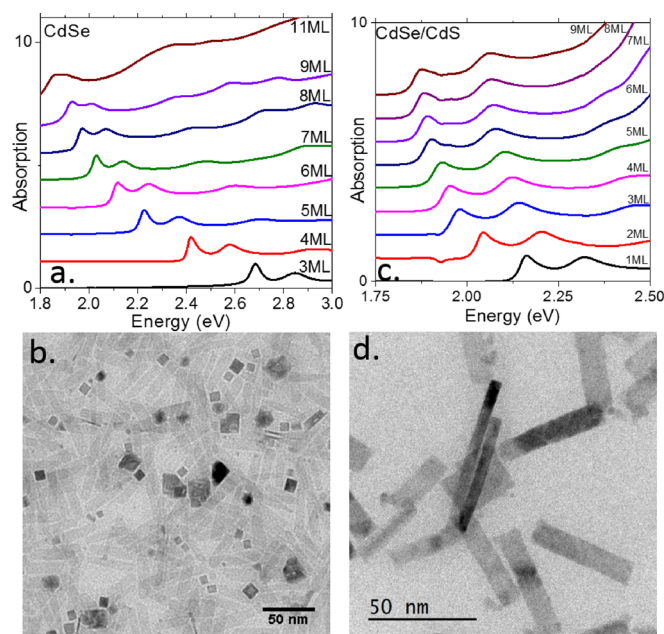

FIG. 1. (a) Absorption spectra of CdSe NPLs with different thicknesses. The spectra have been shifted for clarity. (b) TEM image of the CdSe NPLs with 4 MLs. (c) Absorption spectra of CdSe/CdS NPLs with different thicknesses of the shell. The CdSe core has a thickness of 4 MLs. The spectra have been shifted for clarity. (d) TEM image of the CdSe/CdS NPLs with 4 MLs in the core and 3 MLs in the shell.

TABLE I. Material parameters used for the simulation for CdS, CdSe, and CdTe.

Material	Bulk band gap (eV)	Lattice parameter (nm)
CdS	2.4	0.582
CdSe	1.7	0.608
CdTe	1.5	0.648

For each band, m*(z) and V(z) are equation inputs. In the case of core-only object, the band profile is a square well. The surrounding medium is modeled using a 2 eV offset which is a typical value reported for the transport band offset in nanocrystal arrays.[31] The length of the external barrier is set equal to 2 nm on each side. In a first step, we optimize the effective masses of the homomaterials. The electron effective mass (m_c) is typically tuned from 0 to 0.5 m_0, while the heavy hole effective mass (m_{hh}) is tuned from 0.1 to 1 m_0. For each couple (m_c, m_{hh}), we calculate the interband energy transition. For a given material, we then minimize the quantity $M(m_c, m_{hh}) = \sum_{thickness} (E_{th}(L) - E_{exp}(L))^2$ where L is the thickness of the NPL, E_{exp} is the experimental value for the band edge transition, and E_{th} is the value obtained from the shooting method. The couple (m_c, m_{hh}) which minimizes the value of M is then used for simulation of this material [see Figs. 2 and S4 (supplementary material)]. A typical fit of the experimental data for the homomaterials is given in Fig. 3(b) for CdSe and in Fig. S2 (supplementary material) for other materials. Due to the asymmetry of the electron and hole masses ($m_e < m_h$) in cadmium chalcogenides compounds, the determined electron mass is more critical than the one from the hole [see Fig. S3 (supplementary material)]. When experimental data are available (i.e., for CdSe and CdTe), we also conduct the same set of simulation for the light hole to conduction band transition and determine the light-hole mass. The results are summarized in Table II and will be of utmost interest for future simulations. The results are also compared with the effective masses obtained using the k·p analytical method,[12] and once again, a good correlation is obtained in spite of the strong difference between the two methods.
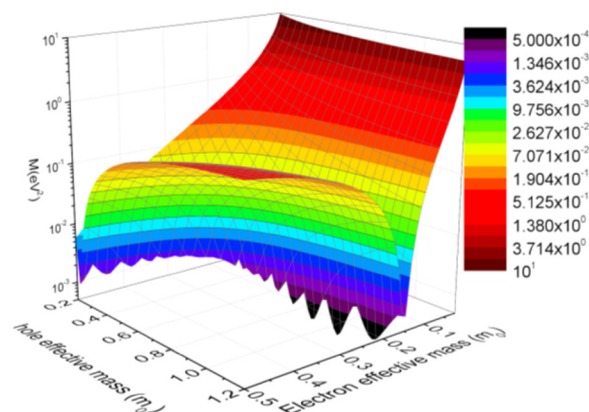

FIG. 2. 3D map of the value of the M matrix as a function of the electron and hole effective masses for a CdSe NPL.
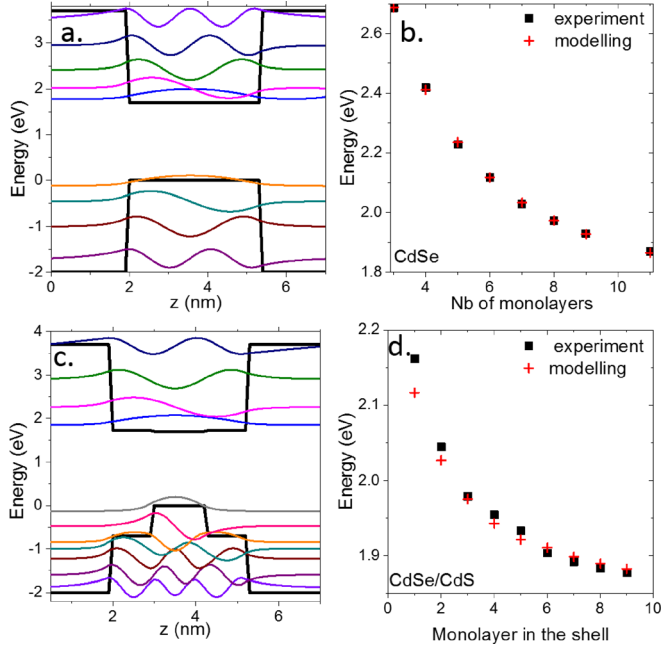
FIG. 3. (a) Energy profile for the conduction and valence bands (black lines) as well as the different wavefunctions for a CdSe NPL. Wavefunctions are shifted at their eigen energy. (b) Energy of the band edge transition (heavy hole to conduction band transition) as a function of the CdSe core thickness. (c) Energy profile for the conduction and valence bands (black lines) as well as the different wavefunctions for a CdSe/CdS NPL. Wavefunctions are shifted at their eigen energy. (d) Energy of the band edge transition (heavy hole to conduction band transition) as a function of the CdS shell thickness. The CdSe core has a thickness of 4 MLs.

In a second step, we optimize the band offset for the CdSe/CdS heterostructure. In this case, we use a constant thickness for the core (4 MLs) and tune the shell thickness. The effective masses are taken equal to those previously determined. A similar least squares fit procedure is used, while the valence band offsets are tuned to minimize the difference between the experimental and shooting method band edge energy gap. The obtained results are given in Figs. 3(c) and 3(d). A good correlation is obtained as long as the shell thickness is above 3 MLs. We obtain a valence band offset of 0.7 eV between CdS and CdSe, while the conduction bands are almost resonant (20 meV offset). The obtained parameters agree well with the commonly admitted picture of a confined hole and a delocalized electron in CdSe/CdS core shell nanocrystals.[32]

B. Exciton binding energy

Once an exciton is formed, the coulombic interaction between the electron and the hole might induce a significant renormalization of the band gap. To account for this effect,

TABLE II. Values of conduction, heavy hole, and light hole effective masses for CdS, CdSe, and CdTe NPLs.

Material	m_c^*	m_c^* k·p[12]	m_{hh}^*	m_{hh}^* k·p[12]	M_{lh}^*	M_{lh}^* k·p[12]
CdS	0.37	0.31	0.41	0.95	-	0.23
CdSe	0.17	0.18	0.9	0.89	0.36	0.19
CdTe	0.12	0.11	0.96	0.49	0.31	0.1

the previously used hamiltonian needs to be corrected by a Coulombic term: $H \rightarrow H_{band\,profile} - \frac{e^2}{4\pi\varepsilon r}$ with ε the dielectric constant taken equal to $10\,\varepsilon_0$ and r the electron hole distance. The two-body wavefunction is taken as the product $\Psi = \xi_e(z_e)\xi_h(z_h)\Psi_r$, where ξ_e/ξ_h are the electron and hole wavefunctions, respectively, previously determined in the absence of coulombic coupling, while Ψ_r relates to the relative motion of electrons and holes. For 1s exciton, the trial function[33] can be used $\Psi_r(r) = \sqrt{\frac{2}{\pi}}\frac{1}{r}\exp(-r/\lambda)$ with λ a variational parameter which plays the role of the Bohr radius. The binding energy E_B of the exciton is then estimated as $E_B = -\frac{\hbar^2}{2\mu\lambda^2} + \frac{e^2}{4\pi\varepsilon}\int\int dz_e dz_h 2\pi r dr \frac{|\Psi_e(z_e)|^2|\Psi_h(z_h)|^2|\Psi_r|^2}{\sqrt{r^2+(z_e-z_h)^2}}$. The value of λ is tuned to maximize E_B (and minimize the total energy); see Fig. 4. We obtain a value of ≈ 50 meV in the case of the CdSe/CdS heterostructure with a Bohr radius of 2.8 nm, which agrees quite well with other perturbative approaches in the absence of dielectric confinement.[25] Such values are consistent with previously reported[13] values of binding energy for 2D CdSe nanoplatelets and are significantly higher than the value reported for the bulk material which highlights the specificity of the 2D geometry. In particular, such large binding energy is responsible for the fast PL lifetime observed in the nanoplatelets[12] compared to their 0D objects and also for the need to apply a large electric field to efficiently dissociate photogenerated electron-hole pairs in NPLs based photodetectors.[9]

However, from a spectral point of view, this binding energy correction is mostly canceled out by the self-energy term,[13] that is why in the following we will only consider the confinement contribution. Thanks to the determined effective parameters (m* and ΔV), it is now possible to simulate the electronic spectrum of a CdSe/CdS NPL. We investigate how the deviation from an ideal band profile is affecting the spectrum of the material. Typically, two effects are discussed in the following part: (i) the effect of the electric field, and (ii) the effect of non-sharp interfaces to consider the effect of gradient interfaces.
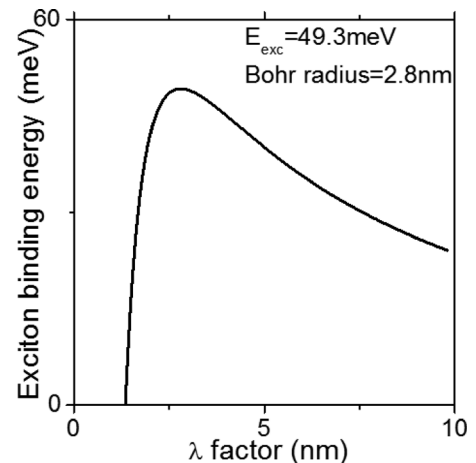

FIG. 4. Exciton binding energy as a function of the λ variational parameter. The Bohr radius corresponds to the value of λ which maximizes the binding energy (and minimizes the total energy).

C. Effect of the electric field

NPLs used for optoelectronic devices (diode, photodetector modulator) are actually operated under an electric field and the latter is expected to bring some modification (Stark effect) of the spectrum which have to be considered at the design level. The modification of the energy profile caused by the addition of an electric field F follows the equation: $V(z, F) = V(z, F = 0) + eFz$, also see in Fig. 5(a). As the structure gets biased, the wavefunctions tend to locate in the triangular part of the quantum well. This leads to a redshift (i.e., reduction of the band edge energy) of the transition known as Stark effect. We quantized this redshift as a function of the applied electric field [see Fig. 5(b)]. The shift estimation is conducted for an NPL with the electric field along the thickness. Noticeable shift (>1 meV) only appears if an electric field above $100 \, \text{kV cm}^{-1}$ gets applied. The determined shifts are in good agreement with experimental values[34–36] obtained for CdSe NPLs where the stark shift can reach a few meV under electric fields of $100–200 \, \text{kV cm}^{-1}$. The predicted shift also follows the expected quadratic dependence for a quantum well, according to the equation: [37]

$$E_{BE}(z, F) = E_{BE}(z, F) - \frac{2^9}{3^5 \pi^6} \frac{e^2 L^4 (m_c + m_{hh})}{\hbar^2} F^2$$ [see Fig. 5(b)]. In

this case, the fitted thickness (L) is 2.7 nm and corresponds to the effective confinement scale probed by the exciton. This value is an intermediate value between the confinement length for electron (core $+ 2 \times$ shells: 3.2 nm) and for the hole (core only: 1.2 nm).

To boost the effect of the electric field, for example, to design a light modulator, a thicker object will be required according to the L^4 scaling of the dependence of the stark shift. This also explains why current measurements based on thin-core objects only show small shifts.[34–36] On the other hand, to build a structure poorly sensitive to the electric field, one should use a more confined profile, where the ground state has an energy which stays far above the triangular part of the energy profile.

D. Effect of non-sharp interfaces

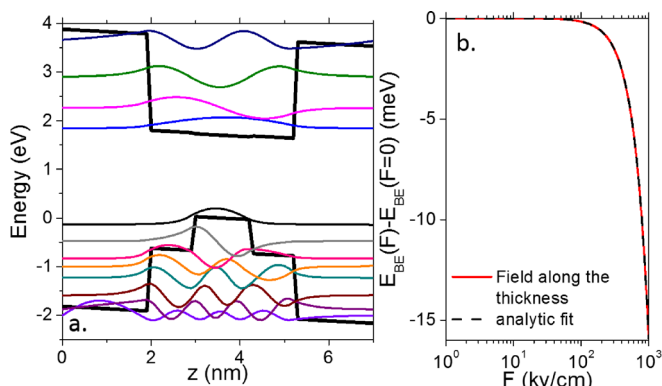Finally, we discuss the effect of non-sharp interfaces. This has attracted a lot of interest recently[38,39] because it has been predicted that smooth interfaces may lead to a reduced Auger effect and thus to a reduced blinking.[40] On III–V semiconductor devices, the physical origin of the non-sharp interfaces is typically different (opening of MBE shutter, material interdiffusion). It is particularly known that smooth interfaces lead to some deviation of the quantum cascade laser spectrum with respect to the originally designed structure.[17] To model this effect in the case of II–VI semiconductor NPLs, we replace the abrupt profile by the following profile: $V(z) = V_b \left(1 - 1/2 \sum_{well} erf \left(\frac{z - Z_r}{L_d} \right) - erf \left(\frac{z - Z_l}{L_d} \right) \right)$, where *erf* is the error function, L_d describes the broadening of the interface, and Z_r and Z_l are the right and left position of the interface for a given well, respectively. A typical profile is given in Fig. 6(a). Here, we investigate a range of broadening which remains in the small perturbation range: the bottom of the sharp profile is still reached in the center of the well. This typically corresponds to the case of the grown heterostructure such as that described in Sec. II. High resolution TEM coupled with Energy dispersive X-ray spectroscopy (EDX) indeed reveals sharp interfaces.[41] More drastic gradient interfaces will actually behave as an alloy and can be obtained experimentally by a long, high temperature (350–400 °C) annealing of the nanocrystals[39] or from a mixed injection of compounds during the growth.

A smooth profile leads to a blueshift of the (inter)band edge transition [see Fig. 6(b)]. It is worth noting that the delocalized character of the electron wavefunction in the case of CdSe/CdS makes the spectrum of the heterostructure actually poorly sensitive to the broadening of this interface. It is also interesting to note that a redshift of the conduction intraband transition is expected [see Fig. 6(c)]. This difference of behavior between the interband and intraband

FIG. 5. (a) Energy profile for the conduction and valence bands in the presence of an electric field ($F = 500 \, \text{kV/cm}$) as well as the different wavefunctions for a CdSe/CdS NPL. Wavefunctions are shifted at their eigen energy. (b) Shift of the band edge energy as a function of the electric field for the NPL thickness in the electric field direction.
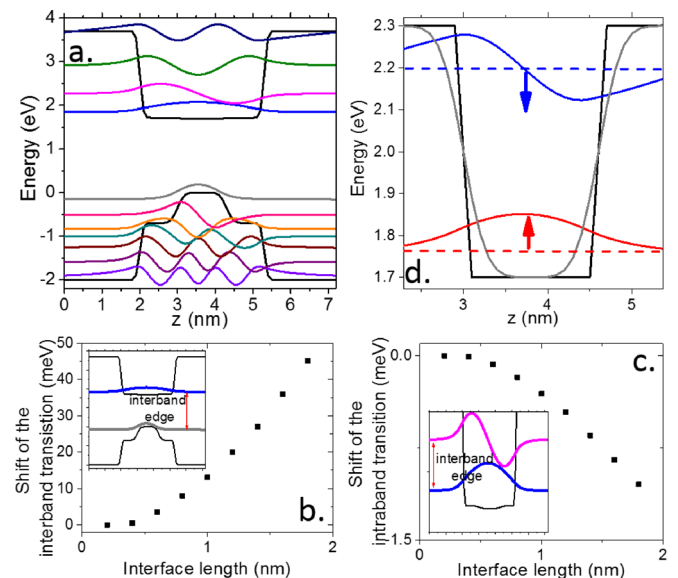

FIG. 6. (a) Energy profile for the conduction and valence bands in the presence of non-abrupt interfaces as well as the different wavefunctions for a CdSe/CdS NPL. Shift of the interband [1Sh-1Se, (b)] and intraband [1Se-1Pe, (c)] transitions as a function of the spreading of the interface. The inset highlights the followed transition (d). Energy profile for the conduction band of a quantum well including two states within the well with a sharp or smooth interface.

transitions can be understood using Fig. 6(d). The states close to the bottom of the band get more confined and their energies are increased. On the other hand, states close to the top of the band get less confined and see their energies decrease.

A possible strategy to make the structure poorly sensitive to the broadening of the interface will be to locate the state at half the confinement energy. However, this is difficult to achieve simultaneously for electrons and holes and the lightest carrier has to be favored.

V. CONCLUSION

We have grown a series of 2D cadmium chalcogenides NPLs with various thicknesses and compared their spectra to our simulation based on 1D resolution of the Schrödinger equation. From this simulation, we have been able to determine a realistic set of effective masses and band offset parameters which will be useful for future simulation and physical property modeling. Then, we have quantized the robustness of the CdSe/CdS heterostructure toward certain modifications such as the application of an electric field, and non-sharp interfaces. In each case, we provide a strategy to enhance or reduce the effects.

SUPPLEMENTARY MATERIAL

See supplementary material which includes experimental energies for CdS, CdSe, CdTe, and CdSe/CdS NPLs, as well as details about the shooting method and effective mass determination.

ACKNOWLEDGMENTS

[1]M. Nasilowski, B. Mahler, E. Lhuillier, S. Ithurria, and B. Dubertret, Chem. Rev. **116**, 10934 (2016).
[2]E. Lhuillier, S. Pedetti, S. Ithurria, B. Nadal, H. Heuclin, and B. Dubertret, Acc. Chem. Res. **48**, 22 (2015).
[3]A. W. Achtstein, A. Antanovich, A. Prudnikau, R. Scott, U. Woggon, and M. Artemyev, J. Phys. Chem. C **119**, 20156 (2015).
[4]M. D. Tessier, C. Javaux, I. Maksimovic, V. Loriette, and B. Dubertret, ACS Nano **6**, 6751 (2012).
[5]A. Riedinger, F. D. Ott, A. Mule, S. Mazzotti, P. N. Knüsel, S. J. P. Kress, F. Prins, S. C. Erwin, and D. J. Norris, Nat. Mater. **16**, 743 (2017).
[6]B. Guzelturk, Y. Kelestemur, M. Olutas, S. Delikanli, and H. Volkan Demir, ACS Nano **8**, 6599 (2014).
[7]J. Q. Grim, S. Christodoulou, F. Di Stasio, R. Krahne, R. Cingolani, L. Manna, and I. Moreels, Nat. Nanotechnol. **9**, 891 (2014).
[8]C. She, I. Fedin, D. S. Dolzhnikov, A. Demortiere, R. D. Schaller, M. Pelton, and D. V. Talapin, Nano Lett. **14**, 2772 (2014).
[9]E. Lhuillier, J. F. Dayen, D. O. Thomas, A. Robin, B. Doudin, and B. Dubertret, Nano Lett. **15**, 1736 (2015).
[10]E. Lhuillier, A. Robin, S. Ithurria, H. Aubin, and B. Dubertret, Nano Lett. **14**, 2715 (2014).
[11]E. Lhuillier, S. Ithurria, A. Descamps-Mandine, T. Douillard, R. Castaing, X. Z. Xu, P.-L. Taberna, P. Simon, H. Aubin, and B. Dubertret, J. Phys. Chem. C **119**, 21795 (2015).
[12]S. Ithurria, M. D. Tessier, B. Mahler, R. Lobo, B. Dubertret, and A. L. Efros, Nat. Mater. **10**, 936 (2011).
[13]R. Benchamekh, N. A. Gippius, J. Even, M. O. Nestoklon, J. M. Jancu, S. Ithurria, B. Dubertret, A. L. Efros, and P. Voisin, Phys. Rev. B **89**, 035307 (2014).
[14]H. Cruguel, C. Livache, B. Martinez, S. Pedetti, D. Pierruci, E. izquierdo, M. Dufour, S. Ithurria, H. Aubin, A. Ouerghi, E. Lacaze, M. G. Silly, B. Dubertret, and E. Lhuillier, Appl. Phys. Lett. **110**, 152103 (2017).
[15]E. Lhuillier, N. Pere-Laperne, I. Ribet-Mohamed, E. Rosencher, G. Patriarche, A. Buffaz, V. Berger, A. Nedelcu, and M. Carras, J. Appl. Phys. **107**, 123110 (2010).
[16]H. Schneider and H. C. Liu, *Quantum Well Infrared Photodetectors, Physics and Applications* (Springer, Heidelberg, 2006).
[17]B. Schwarz, C. A. Wang, L. Missaggia, T. S. Mansuripur, P. Chevalier, M. K. Connors, D. McNulty, J. Cederberg, G. Strasser, and F. Capasso, ACS Photonics **4**, 1225 (2017).
[18]E. Lhuillier, I. Ribet-Mohamed, E. Rosencher, G. Patriarche, A. Buffaz, V. Berger, and M. Carras, Appl. Phys. Lett. **96**, 061111 (2010).
[19]A. W. Achtstein, R. Scott, S. Kickhöfel, S. T. Jagsch, S. Christodoulou, G. H. V. Bertrand, A. V. Prudnikau, A. Antanovich, M. Artemyev, I. Moreels, A. Schliwa, and U. Woggon, Phys. Rev. Lett. **116**, 116802 (2016).
[20]S. Bose, Z. Song, W. J. Fan, and D. H. Zhang, J. Appl. Phys. **119**, 143107 (2016).
[21]A. W. Achtstein, A. Schliwa, A. Prudnikau, M. Hardzei, M. V. Artemyev, C. Thomsen, and U. Woggon, Nano Lett. **12**, 3151 (2012).
[22]W. Sukkabot, J. Comput. Electron. **16**, 796 (2017).
[23]F. Thierry, J. Le Rouzo, F. Flory, G. Berginc, and L. Escoubas, J. Nanophotonics **9**, 093080 (2015).
[24]P. Harrison, *Quantum Wells, Wires and Dots: Theoretical and Computational Physics of Semiconductor Nanostructures*, 2nd ed. (Wiley-Interscience, 2005).
[25]F. Rajadell, J. I. Climente, and J. Planelles, Phys. Rev. B **96**, 035307 (2017).
[26]A. Polovitsyn, Z. Dang, J. L. Movilla, B. Martin-Garcia, A. Hossain Khan, G. H. V. Bertrand, R. Brescia, and I. Moreels, Chem. Mater. **29**, 5671 (2017).
[27]A. A. Rossinelli, A. Riedinger, P. Marqués-Gallego, P. N. Knüsel, F. V. Antolinez, and D. J. Norris, Chem. Commun. **53**, 9938 (2017).
[28]A. Antanovich, A. Achtstein, A. Matsukovich, A. Prudnikau, P. Bhaskar, V. Gurin, M. Molinari, and M. Artemyev, Nanoscale **9**, 18042 (2017).
[29]S. Pedetti, B. Nadal, E. Lhuillier, B. Mahler, C. Bouet, B. Abécassis, X. Xu, and B. Dubertret, Chem. Mater. **25**, 2455 (2013).
[30]S. Ithurria and D. V. Talapin, J. Am. Chem. Soc. **134**, 18585 (2012).
[31]Y. Liu, M. Gibbs, J. Puthussery, S. Gaik, R. Ihly, H. W. Hillhouse, and M. Law, Nano Lett. **10**, 1960 (2010).
[32]M. Marceddu, M. Saba, F. Quochi, A. Lai, J. Huang, D. V. Talapin, A. Mura, and G. Bongiovanni, Nanotechnology **23**, 015201 (2012).
[33]C. P. Hilton, W. E. Hagston, and J. E. Nicholls, J. Phys. A **25**, 2395 (1992).
[34]N. V. Tepliakov, I. O. Ponomareva, M. Yu. Leonov, A. V. Baranov, A. V. Fedorov, and I. D. Rukhlenko, J. Phys. Chem. C **120**, 2379 (2016).
[35]R. Scott, A. W. Achtstein, A. V. Prudnikau, A. Antanovich, L. D. A. Siebbeles, M. Artemyev, and U. Woggon, Nano Lett. **16**, 6576 (2016).
[36]A. W. Achtstein, A. V. Prudnikau, M. V. Ermolenko, L. I. Gurinovich, S. V. Gaponenko, U. Woggon, A. V. Baranov, M. Yu. Leonov, I. D. Rukhlenko, A. V. Fedorov, and M. V. Artemyev, ACS Nano **8**, 7678 (2014).
[37]E. Rosencher and B. Vinter, *Optoelectronics*, 2nd ed. (Cambridge University Press, 2002).
[38]Y.-S. Park, W. K. Bae, L. A. Padilha, J. M. Pietryga, and V. I. Klimov, Nano Lett. **14**, 396 (2014).
[39]M. Nasilowski, P. Spinicelli, G. Patriarche, and B. Dubertret, Nano Lett. **15**, 3953 (2015).
[40]G. E. Cragg and A. L. Efros, Nano Lett. **10**, 313 (2010).
[41]B. Mahler, B. Nadal, C. Bouet, G. Patriarche, and B. Dubertret, J. Am. Chem. Soc. **134**, 18591 (2012).
[42]Z. Li, H. Qin, D. Guzun, M. Benamara, G. Salamo, and X. Peng, Nano Res. **5**, 337 (2012).